MATHAUS HENRIQUE DA SILVA ALVES

RESEARCH OF THE STRUCTURAL, ELECTRONIC, AND MECHANICAL PROPERTIES OF NEW PALLADIUM-BASED SULFOSALTS UNDER HIGH PRESSURE

LAVRAS – MG

2022

MATHAUS HENRIQUE DA SILVA ALVES

RESEARCH OF THE STRUCTURAL, ELECTRONIC, AND MECHANICAL PROPERTIES OF NEW PALLADIUM-BASED SULFOSALTS UNDER HIGH PRESSURE

Dissertation thesis presented to the Federal University of Lavras as part of the Graduate Program in Physics requirements, concentration area in Condensed Matter Physics, to obtain the Master's title.

Prof. Dr. Raphael Longuinhos Monteiro Lobato
Orientador

Prof. Dra. Jenaina Ribeiro Soares
Coorientadora

LAVRAS – MG
2022

Ficha catalográfica elaborada pelo Sistema de Geração de Ficha Catalográfica da Biblioteca Universitária da UFLA, com dados informados pelo(a) próprio(a) autor(a).

Alves, Mathaus Henrique da Silva
Research of the Structural, Electronic, and Mechanical Properties of New Palladium-based Sulfosalts Under High Pressure / Mathaus Henrique da Silva Alves. - 2022.
42 p. : il.

Dissertação (mestrado acadêmico)–Universidade Federal de Lavras, 2022.
Orientador: Raphael Longuinhos Monteiro Lobato.
Coorientadora: Jenaina Ribeiro Soares.
Bibliografia.

1. DFT. 2. New Materials. 3. High Pressure. I. Lobato, Raphael Longuinhos Monteiro. II. Soares, Jenaina Ribeiro. III. Título.

MATHAUS HENRIQUE DA SILVA ALVES

RESEARCH OF THE STRUCTURAL, ELECTRONIC, AND MECHANICAL PROPERTIES OF NEW PALLADIUM-BASED SULFOSALTS UNDER HIGH PRESSURE

ESTUDO DAS PROPRIEDADES ESTRUTURAIS, ELETRÔNICAS E MECÂNICAS DE NOVOS SULFOSSAIS À BASE DE PALÁDIO SOB ALTAS PRESSÕES

Dissertation thesis presented to the Federal University of Lavras as part of the Graduate Program in Physics requirements, concentration area in Condensed Matter Physics, to obtain the Master's title.

APPROVED on November 08, 2022.

Prof. Dr. Moises Porfirio Rojas Leyva	UFLA
Prof. Dr. Paulo Alliprandini Filho	UFVJM

Prof. Dr. Raphael Longuinhos Monteiro Lobato
Orientador

Prof. Dra. Jenaina Ribeiro Soares
Coorientadora

LAVRAS – MG
2022

This work is dedicated to possible readers. I hope you make your dreams come true.

ACKNOWLEDGEMENTS

Special thanks to the UFLA's Physics Graduate program, UFLA's department of physics (DFI), and UFLA professors for providing me with quality education and support.

I am also grateful to UFVJM for quality education and growth opportunities.

I am deeply indebted to my advisors, Raphael Longuinhos and Jenaina Ribeiro, for the guidance and the knowledge transmitted during this period; it was hard work, but "you guys" showed me "the rocky road to professional growth" ("caminho das pedras" in Portuguese). No doubt great researchers.

Thank also to professors Cleverson Filgueiras, Cleber Anconi, Robson Armindo, and Rodrigo Bufalo for accepting the invitation to the qualification exam and for the corrections pointed out.

I am grateful to professor and coordinator Rodrigo Bufalo, for their cordiality and help with questions regarding technical issues of the UFLA graduate program (seriously, this "guy" knows everything about the program).

I am grateful to professors Moises Leyva and Paulo Alliprandini for the scientific-technical analysis of this text, pointing out corrections and suggestions.

I could not have undertaken this journey without the love and affection of my family (Maria Sueli, Lara, Camila, Idenilson, Augusta e Conceição) and my friends. If it were not for them, I would not be here.

Don’t wait: the time will never be "the right time."
(Napoleon Hill)

ABSTRACT

Pressure is a fundamental thermodynamic variable that can be used to modify the properties of materials because it reduces the interatomic distances and modifies the electronic orbitals and the connection patterns of the sample. It is a versatile tool for creating exotic materials not accessible in environmental conditions. Recently, high-pressure experimental techniques developed have led to the synthesis of new functional materials with excellent performance: for example, superconductors, superhard materials, and high energy density materials. Computer simulations aided and accelerated some of these advances, an essential tool for the search for crystalline structures and the characterization of physical properties. Thus, this work investigated the structural, electronic, and mechanical properties of the *Roterbärite* family ($PdCuBiX_3$ - $X = S$, Se or Te) under the influence of high pressure through Density Functional Theory (DFT) calculations using the Quantum Espresso. The calculations have been performed using Perdew–Zunger's LDA (LDA-PZ) exchange-correlation (XC) functional. The crystal structure has been computationally optimized under several pressures, and the bulk modulus was found to be 71,65 GPa, 53,02 GPa, and 50,3 GPa for the $PdCuBiS_3$, $PdCuBiSe_3$ and $PdCuBiTe_3$ respectively. Electronic structure calculations demonstrated that $PdCuBiS_3$ and $PdCuBiSe_3$ are semiconductors, and $PdCuBiTe_3$ is metallic.

Keywords: DFT, electronic structure, bulk modulus, new materials, high-pressure.

RESUMO

A pressão é uma variável termodinâmica fundamental que pode ser utilizada para controlar as propriedades dos materiais, pois, ela reduz as distâncias interatômicas, modifica os orbitais eletrônicos e os padrões de ligações das amostras. É uma ferramenta versátil para a criação de materiais exóticos não acessíveis em condições ambientais. Recentemente, técnicas experimentais de altas pressões levaram à síntese de novos materiais funcionais com excelentes desempenhos. Como por exemplo: supercondutores, materiais superduros e materiais de alta densidade de energia. Alguns desses avanços foram auxiliados e acelerados por simulações computacionais, uma importante ferramenta para a busca de estruturas cristalinas e caracterização das propriedades físicas. Com isso, este estudo busca investigar as propriedades estruturais, eletrônicas e mecânicas dos minerais da família da *Roterbärite* ($PdCuBiX_3$ - $X = S$, Se or Te) sob influência de altas pressões através de cálculos via Teoria do Funcional da Densidade (DFT) usando o Quantum Espresso. Os cálculos foram realizados usando o funcional de troca e correlação (XC) LDA de Perdew-Zunger (LDA-PZ). A estrutura cristalina foi otimizada computacionalmente sob várias pressões e os módulos de *bulk* encontrados foram de 71,65 GPa, 53,02 GPa e 50,3 GPa para o $PdCuBiS_3$, $PdCuBiSe_3$ e $PdCuBiTe_3$, respectivamente. Os cálculos de estrutura de bandas demonstraram que $PdCuBiS_3$ e $PdCuBiSe_3$ são semicondutores, e $PdCuBiTe_3$ é metálico.

Palavras-chave: DFT, propriedades eletrônicas, modulo de bulk, novos materiais, altas pressões

LIST OF FIGURES

LIST OF TABLES

CONTENTS

1 INTRODUCTION

1.1 Contextualization

High-pressure physics has developed rapidly in recent decades (RYCHKOV, 2020; TSE, 2019; MAO et al., 2016). It was studying high pressure awarded the 1946 Nobel Prize in Physics to Percy Williams Bridgman due to his outstanding contributions of dramatic improvements in high-pressure apparatuses and measurement techniques (NEWITT, 1962; BECKER, 1961; BRIDGMAN, 1914; HAZEN; HAZEN, 1999). Besides, artificial diamonds were first produced by applying high pressure to carbon (WANG et al., 2020). It was also applying high pressure to the quartz that Coesite and Stishovite were first synthesized in 1953 and 1961, respectively. Both having a natural occurrence in a meteorite impact crater (Meteor Crater (METEOR..., [2021?])) in Arizona, US, were reported by Edward C. T. Chao, the Coesite in 1960 (CHAO; SHOEMAKER; MADSEN, 1960) and the Stishovite in 1962 (FLEISCHER, 1962).

High pressure can generate phase transitions and new phases, creating new chemical reactions with structural transformations of molecules and electronic transitions (KATRUSIAK, 2008). These reactions include synthesizing several exotic compounds inaccessible at ambient conditions, such as superhard materials, noble gases reactions, and superconductors (ZHANG et al., 2017). Predicting the reactions and transformations generated by pressure is difficult. For example, there are stable gas hydrates at high pressure (KUHS, 2004; SHIMIZU et al., 2002). Although most substances become metallic under high pressure, new materials of the superconducting type can be obtained (BUDZIANOWSKI; KATRUSIAK, 2004; KATRUSIAK, 2008). Another example is ice, with 19 crystal structures (polymorphism) obtained at different pressures and temperatures (GASSER et al., 2021).

Pressure can contribute considerably to a better understanding of many condensed-matter phenomena (DUTTA et al., 2019; ZHANG et al., 2021). In recent years, several minerals have been subjected to high pressures seeking to characterize their properties for possible applications in creating electronic devices (HUANG et al., 2019; LI et al., 2020; RAHMAN; HAQUE; HOSSAIN, 2019; DUTTA et al., 2018; ZHANG et al., 2021; LI et al., 2020; KANG et al., 2015).

Furthermore, collaborators at the geology center of the Czech Republic studied and published a paper about an unknown mineral (reported by (CABRAL; LIESSMANN; LEHMANN, 2015)) corresponding to $PdCuBiSe_3$ (VYMAZALOVÁ et al., 2020; VYMAZALOVÁ et al.,

2019). This new mineral is called Roterbärite, a rare compound variant of sulfosalt (BRITANNICA, 2018) Malyshevite ($PdCuBiS_3$) but includes Selenium in the chemical formula instead of Sulfur.

This work aims to study and characterize the structural and electronic properties of Roterbärite and Malyshevite under high pressure through simulation using first principles methods (*ab initio*). In addition, a new undiscovered variant mineral is still proposed, $PdCuBiTe_3$. So it is shown the optimized structural, bulk modulus, and electronic properties by applying high pressures of the three minerals using Density Functional Theory (DFT) theory.

1.2 Objectives

1.2.1 General objective

- DFT calculations to investigate the structural, mechanical, and electronic properties of new minerals ($PdCuBiX_3$ - $X = S$, Se or Te), as well as their modifications by the high-pressure application.

1.2.2 Specific objectives

- Simulation of new materials.
- Geometry optimization at several pressures
- Bulk modulus calculation
- Band structure and Density Of States (DOS) calculation

1.3 The organization this work

Chapter 2 presents the theoretical foundation and describes the main characteristics of the theoretical and computational methods used. This chapter describes the Hamiltonian of many interacting bodies, followed by approximations to make the problem numerically tractable.

In chapter 3, the methodology of this study is presented. Chapter 4 presents and discusses the results obtained from the execution of the methodology. The conclusions related to the results and perspectives for future works are presented in chapter 5.

2 THEORETICAL FOUNDATION

The structural, mechanical, and electronic characterization of atoms, molecules, and condensed phases under high pressure can be studied by two methods:

1. Experimental techniques performed in a Diamond Anvil Cell (DAC), by X-ray diffraction and Raman spectroscopy (ANZELLINI et al., 2019):

   (a) DAC possibilities to generate high pressures of order to multiple Gigapascals GPa in materials, allowing *in situ* measurements of the electrical, elastic, and thermodynamic parameters (including shear modulus, compression velocities, thermal capacity, entropy, kinetic energy, Debye temperature, etc.) (BROWN; MCQUEEN, 1986; MAO et al., 2001). For example, electrical resistance measurements under high pressure can reveal a material as an insulator, semiconductor, metal, or even as a superconductor (HAN et al., 2005). It even provides high-pressure transformation behaviors, allowing the discovery of electronic or structural phase transitions (PATTERSON et al., 2000; VELISAVLJEVIC; VOHRA, 2003).

2. The computational methods can be divided into two groups, the Density Functional Theory (DFT) and the Force Field (FF) (RYCHKOV, 2020):

   (a) The FF method is a semi-empirical computational method used to estimate the forces between atoms within molecules without explicitly considering their electronic structure (RYCHKOV, 2020). This method is implemented, for example, in the software *PIXEL* (GAVEZZOTTI, 2011) and *CrystalExplorer17* (THOMAS et al., 2018; MACKENZIE et al., 2017).

   (b) The DFT method is a first-principles[1] computational modeling method to determine the properties of a multi-electronic system that make up the atoms of a crystal by explicitly treating their electronic structure. In DFT, the primary variable is the electron density of the system, and no longer the multi-electronic wave function as in the case of the Theory of Hartree and Fock (HARTREE, 1928; FOCK, 1930; SLATER, 1951). Examples of packages that implement the

[1] "Ab initio model" or a "first principles model" is a mathematical model about a sufficiently large set of natural phenomena. The physics properties should emerge from the numerical solution of these models (IFIMAC, [201-?l).

DFT are *Quantum Espresso* (GIANNOZZI et al., 2017), *CPMD* (ANDREONI; CURIONI, 2000), *CASTEP* (CLARK et al., 2005) and *CRYSTAL* (DOVESI et al., 2018).

Furthermore, density functional theory has been widely used to study mineral phases' properties (structure, energy, elasticity, etc.) relevant to Earth and Planetary Sciences (OGANOV; BRODHOLT; PRICE, 2002). In addition, this chapter presents a brief introduction to the theory of computer simulation of solids used in this work (DFT).

2.1 Multi-body Problem

In Quantum mechanics, the energy of a system E can be determined by solving the Schrodinger equation (COHEN; MORI-SáNCHEZ; YANG, 2012):

$$\mathscr{H}\Psi = E\Psi, \tag{2.1}$$

where Ψ is the wave function and $\mathscr{H}$ is the Hamiltonian operator. It is interesting to calculate the energy's expectation value, i. e. the probabilistic expected value of the result (measurement) of an experiment (COHEN-TANNOUDJI et al., 2006). Moreover, the expectation value is obtained by knowing the system's wave function. This resolution is only possible by relating Ψ to the boundary conditions of the interest system. In particular, the interaction for many electrons and nucleus (multi-body) without the external potentials is given by the Hamiltonian operator (PARR, 1980):

$$\mathscr{H} = T_e + T_n + W + v + \upsilon, \tag{2.2}$$

where T_e is an electric kinetic energy, W electrons interaction potential with electrons, υ electrons interaction potential with nucleus; T_n is a nucleus kinetic energy, and v nucleus interaction potential. This Hamiltonian can be written in the non-relativistic approximation with the terms expressed in the first quantization and Gaussian units (LOBATO, 2015):

$$\mathscr{H} = \underbrace{\frac{-\hbar^2}{2}\left[\sum_i \frac{\nabla_i^2}{m_e} + \sum_I \frac{\nabla_I^2}{M_I}\right]}_{T_e+T_n} + \underbrace{\frac{1}{2}\sum_{i\neq j}\frac{e^2}{|r_i - r_j|}}_{W} + \underbrace{\frac{1}{2}\sum_{I\neq J}\frac{Z_i Z_j e^2}{|R_i - R_j|}}_{v} - \underbrace{\sum_{i,I}\frac{Z_i e^2}{|r_i - R_I|}}_{\upsilon}, \tag{2.3}$$

where, for the electrons, e is the charge, m_e is the mass, and r_i is its coordinates. For the nucleus, Z_e, M_I, R_I, respectively the same properties are described (LOBATO, 2015).

The study of eq. Equation 2.3 using wave functions for the solve Schrodinger equation is complicated because the increase of electron number this formulation becomes computationally demanding, or even unthinkable[2]. For example, the wave function of benzene depends on 126 electronic coordinates, where this molecule is made up of six carbon, and six hydrogen atoms (HAMMES-SCHIFFER, 2017). On the other hand, the DFT method (section 2.3) is an example of a multi-body system that studies the electronic or nucleus structure, principally the ground state using an electronic density. With this method is possible to get the same information as wave functions but less computationally demanding (BASEDEN; TYE, 2014).

2.2 Borh-Oppenheimer approach

It's complex to work with the previous Hamiltonian (Equation 2.3) because the study of the electronic structure of solids becomes insoluble, even for numerical solutions. It is necessary for some approximations.

The first approach is the Borh-Oppenheimer approach, or adiabatic approximation (BORN; OPPENHEIMER, 1927), and consists of decoupling the electronic coordinates from the nuclear ones, To deal separately the dynamics of the nucleus and the dynamics of electrons. Because the mass of the nucleus is much greater than the mass of the electrons, the nucleus is considered static, and the electrons are moving at an appreciable speed. For most molecular systems, this assumption is accurate (CHELIKOWSKY, 2019).

Thus, the electrons are described by an electron Hamiltonian, H_e, given by (PARR, 1980):

$$\mathscr{H}_e = T_e + W + \upsilon = \frac{-\hbar}{2m_e}\sum_i \nabla_i^2 + \frac{1}{2}\sum_{i\neq j}\frac{e^2}{|r_i - r_j|} - \sum_{i,I}\frac{Z_i e^2}{|r_i - R_I|}. \tag{2.4}$$

This equation (2.4) is more simplified, but its resolution remains difficult. For real systems to be computationally treated, other approaches must be taken into account (KOHN, 1999). These approaches include: Hartree-Fock and DFT (CHELIKOWSKY, 2019).

[2] The Hartree-Fock method is an example of the study quantum many-body for the wave equation in a stationary state (Froese Fischer, 1987).

2.3 Density-functional theory (DFT)

Pioneers works by Thomas and Fermi (THOMAS, 1927; FERMI, 1927) on electronic energy in terms of electron density distribution, $n(r)$ (KOHN, 1999):

$$n(\vec{r}) = N \int |\psi * (\vec{r}_1, \vec{r}_2, ..., \vec{r}_N) \psi(\vec{r}_1, \vec{r}_2, ..., \vec{r}_N)| \times d\vec{r}_2 ... d\vec{r}_N, \tag{2.5}$$

contributed for the starting point of modern DFT. $\psi(\vec{r}_1, \vec{r}_2, ..., \vec{r}_N)$ is a wave function for many electrons and N is a number of the interacting electrons; In this theory, the external potential (υ) is a functional ($F[n(\vec{r})]$) of the ground-state density $n(\vec{r})$). In other words, the observable quantities of an N-electron quantum system are completely determined by the ground state charge density ($n(\vec{r})$) (COHEN; MORI-SáNCHEZ; YANG, 2012). This statement constitutes the Hohenberg Kohn theorems (HOHENBERG; KOHN, 1964):

1. "The electron density determines the external potential (to within an additive constant)."
2. "For any positive definite trial density, n, such that $\int n(\vec{r}) d\vec{r} = N$ then $E[n] \geq E_0$"

With the first theorem, it immediately follows that the electron density uniquely determines the Hamiltonian operator (Equation 2.4). This is because the Hamiltonian is specified by the external potential υ and the total number of electrons, N, which can be calculated from the density simply by integrating across space. Thus, in principle, given the charge density, the Hamiltonian operator could be determined, as well as the wave functions $\psi(\vec{r}_1, \vec{r}_2, ..., \vec{r}_N)$ and the material properties (HARRISON, 2003). Now note that the second theorem establishes a variational principle, where E_0 is the ground state energy. This theorem is restricted to ground-state studies. An extension allows the study of excited states, that can be guaranteed orthogonal to the ground state. Still, to obtain this knowledge, the ground state wave function is needed (HARRISON, 2003).

Notably, using density to solve the Hamiltonian significantly reduces the number of variables and coordinates in the system.

2.4 The Kohn–Sham Equation

In the 1960s, Pierre Hohenberg, Walter Kohn, and Lu Sham established the theoretical framework for justifying the replacement of the many-body wave function by one-electron or-

bitals with the electron density being a key quantity (HOHENBERG; KOHN, 1964; KOHN; SHAM, 1965). As seen in the previous section, Hohenberg and Kohn proposed that the total electronic energy of a system was uniquely dependent on the electron's density. Then, Sham and Kohn provided a recipe for calculating this necessary density. For this work, in 1998, Walter Kohn received the Nobel Prize in Chemistry (KOHN, 1999).

Now to introduce the approximation of Kohn-Sham, it's necessary to review the problem in solving the Hartree-Fock equation, given by (ECHENIQUE; ALONSO, 2007):

$$\left(\frac{-\hbar^2\nabla^2}{2m} + V_N(\vec{r}) + V_H(\vec{r}) + V_x^i(\vec{r})\right)\phi_i(\vec{r}) = E_i\phi_i(\vec{r}), \tag{2.6}$$

where the principal problem is on the exchange term x (of the potential $V_x^i(\vec{r})$) that depends on the orbital i. For example, considering five occupied orbitals the system will have five coupled Hamiltonians. So Kohn and Sham suppose that the exchange potential did not depend on the orbital ($V_x^i = V_x$) reducing the problem from five Hamiltonians to one, by the introduction of the *Local Density Approximation (LDA)* (CHELIKOWSKY, 2019). In this approximation, one will write exchange energy of the system as (KOHN; SHAM, 1965):

$$E_x[n(\vec{r})] = \int n(\vec{r})\mathscr{E}_x[n(\vec{r})]d^3r, \tag{2.7}$$

for an electronic density of n, the term $\mathscr{E}_x[n(\vec{r})]$ is the "exchange energy density". Still, in this theory, the exchange potential is determined from the functional derivative of $E_x[n(\vec{r})]$:

$$V_x[n] = \frac{\delta E_x[n]}{\delta n}. \tag{2.8}$$

So far, one has assumed a general term without specifying $\mathscr{E}_x[n(\vec{r})]$. Well, physicists work with approximations, considering the exchange energy per electron of free electron gas (see section 4.2 of (CHELIKOWSKY, 2019)):

$$\mathscr{E}_x = -\frac{3e^2}{4\pi}k_f = -\frac{3e^2}{4\pi}(3\pi^2 n)^{1/3}, \tag{2.9}$$

making an audacious assumption. I. e., the previous exchange energy density (free electron gas) is a universal functional applicable to all electronic structure problems. It can be written as:

$$E_x[\rho] = -\frac{3e^2}{4\pi}(3\pi^2)^{1/3}\int [n(\vec{r})]^{4/3}d^3r, \tag{2.10}$$

or using eq. 2.8, is obtained:

$$V_x[n] = -\frac{e^2}{\pi}(3\pi^2 n(\vec{r}))^{1/3}. \tag{2.11}$$

About 15 years before Kohn and Sham's work, Slater obtained a similar equation differing by a factor of 2/3 from the previous equation. However, Slater minimized the system's energy using the average of the free electrons, while Kohn and Sham used the functional density (ASHCROFT; MERMIN et al., 1976).

One can also consider the total density in terms of the density of electrons spin-up and electrons spin-down. This approach is known *Local Spin Density Approximation (LSDA)*, and the functionals of this approximation treat "up" and "down" spin differently.

With that, given a functional exchange and correlation for the electronic structure of matter, it can be solved the Kohn–Sham equation (with the "self-consistently" method (CHELIKOWSKY, 2019)):

$$\left(\frac{-\hbar^2\nabla^2}{2m} + V_N(\vec{r}) + V_H(\vec{r}) + V_{xc}[n(\vec{r})]\right)\phi_i(\vec{r}) = E_i\phi_i(\vec{r}). \tag{2.12}$$

Once a self-consistent solution of the Kohn–Sham equation is obtained, the total energy can be computed from:

$$E_{KS} = \sum_i^M -1/2\int \rho(\vec{r})V_H(\vec{r})d^3r + \int \rho(\vec{r})(\mathscr{E}_{xc}[\rho(\vec{r})] - V_{xc}[\rho(\vec{r})])d^3r. \tag{2.13}$$

The DFT solution for the energies in the considered system is exact in principle. However, the nature of the many-body electronic interaction is mapped to an exchange and correlation potential ($V_{xc}[\rho(\vec{r})]$) that needs to be approximated, according to the Kohn-Sham approximation.

2.5 The Pseudopotential Approximation

It is known that in the bonds of chemical elements, only valence electrons participate in them. For example, the carbon atom has electron configuration $1s^2 2s^2 2p^2$. The 1s state is tightly bound and highly localized around the nucleus. Furthermore, the $1s$ state is not strongly altered when carbon atoms form bonds. Instead, a combination of the $2s$ and $2p$ states is known to form a chemical bond. Another example of the role of electronic valence states is the element

sodium, which has an atomic configuration of $1s^2 2s^2 2p^6 3s^1$. The $1s^2 2s^2 2p^6$ electronic states are tightly bound and do not contribute to metallic bonds in solid elemental sodium. Only the $3s1$ electron moves through the sodium crystal to carry current.

Strongly bounded, more internal electronic states are called "core states," and outermost, weakly bounded electronic states are called "valence states." Valence states are recognized in the periodic table, and elements are grouped into columns based on that.

Can this physical idea of valence and central states be incorporated into a workable approximation to help us solve the Kohn-Sham equation?

Differently treating core and valence states is a good idea. Although the Kohn-Sham equation is much simpler than the Hartree-Fock description, the problem still needs to be solved. The properties of small molecules with light elements are decidedly more straightforward to calculate than large molecules with heavy elements. Heavy elements have more complex wave functions due to the many electrons. For example, the solution of the Kohn-Sham equation for a *Pb* atom is approximately 2500 times more difficult to solve than for a *C* atom considering only the number of electrons (CHELIKOWSKY, 2019).

One of the first researchers to solve this problem was Hellmann (HELLMANN, 1935), who suggested treating the electronic states of an atom in two terms. The valence electrons, first term, interact to form bonds, and the nucleus electrons, second term, remain inert. An image of the matter according to Hellmann's ideas is shown in Fig. 2.1

With this model, electrons bonded more strongly to the nucleus, called "core" electrons, unite with the nucleus, forming a single nucleus, called a pseudonucleus. With this in mind, the atom or pseudoatom is formed by the pseudonucleus and valence electrons (pseudovalence). These perceive pseudopotential rather than real potential.

Thus, it is possible to describe the real potential of a system through a pseudopotential that ideally provides the same results from a cutoff radius r_c, which is described approximately on a plane wave basis (ZIMAN, 1972).

Fig. 2.2 is shown a Coulomb potential and its wave function in blue compared to the pseudopotential in red. The real wave function and the pseudo wave and potentials combine after a certain cutoff radius.

This theory makes it possible to study molecular systems more efficiently.

Figura 2.1 – Hellmann's pseudopotential model.

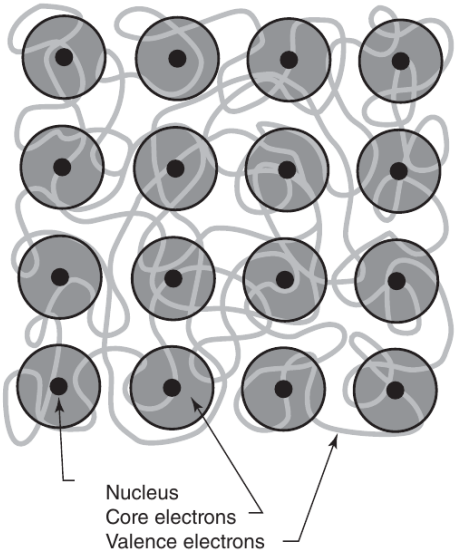

Label: The valence electrons move in a fixed arrangement of chemically inert ion cores. The ion cores are composed of the nucleus and core electrons.

Source: (CHELIKOWSKY, 2019).

Figura 2.2 – Comparison of pseudopotential with real potential.

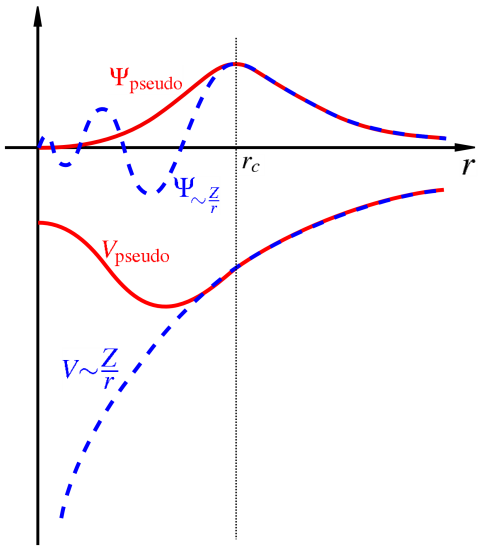

Source: (WIKEMEDIA. . . , 2006).

2.6 Introduction to Crystals

In general, solids can be classified as crystalline and amorphous according to the spatial distribution of atoms, molecules, or ions. An amorphous solid is composed of atoms, molecules, or ions that do not show a long-range ordering. A crystalline solid or crystal is formed by a periodic arrangement of identical units, atoms, groups of atoms, molecules, or ions, arranged

in a repetitive, containing a small number of imperfections and impurities (AVERILL, 2021; LOWER, 2017).

On the other hand, an ideal crystal is a perfect, infinite repetition of identical groups of atoms. These groups are called the base of the crystal. A crystal lattice is a set of mathematical points associated with the base of the crystal. These points are associate a primitive translation vectors, $\vec{a}_1$, $\vec{a}_2$ and $\vec{a}_3$ (KITTEL; MCEUEN; MCEUEN, 1996; ASHCROFT; MERMIN et al., 1976).

Primitive translation vectors are often used to define the crystalline axes of a primitive parallelepiped. This parallelepiped is called a primitive cell, the smallest unit cell possible (Fig. 2.3). A unit cell, not necessarily primitive, can fill all space through appropriate translations (RÖSSLER, 2009; KITTEL; MCEUEN; MCEUEN, 1996).

Figura 2.3 – Three-dimensional lattice of a primitive cell.

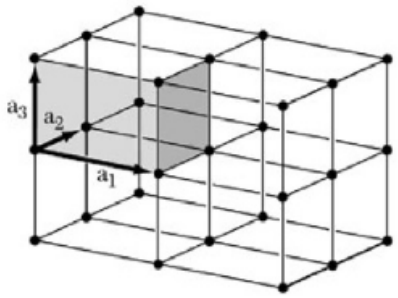

Source: (KITTEL; MCEUEN; MCEUEN, 1996).

Note that the complete description of the unit cell consists of the representation of the spatial part by the network parameters a, b, and c, in which you determine the cell's dimensions employing axes or edges. Thus, these parameters are related to the alpha, beta, and gamma angles formed between the network parameters. The distribution of symmetry points in the respective volume created by the network parameters also describes the unit cell based on symmetry operations: **reflection, rotation, or inversion** (SYMMETRY. . . , 2019; NELSON, 2013).

Unit cells are determined by 230 symmetry groups grouped into 14 possible structures that make up the 7 existing crystal systems called Bravais lattices, see figure 2.4 (AROYO, 2016; WHAT. . . , [201-?l).

Figura 2.4 – The Bravais Lattices.

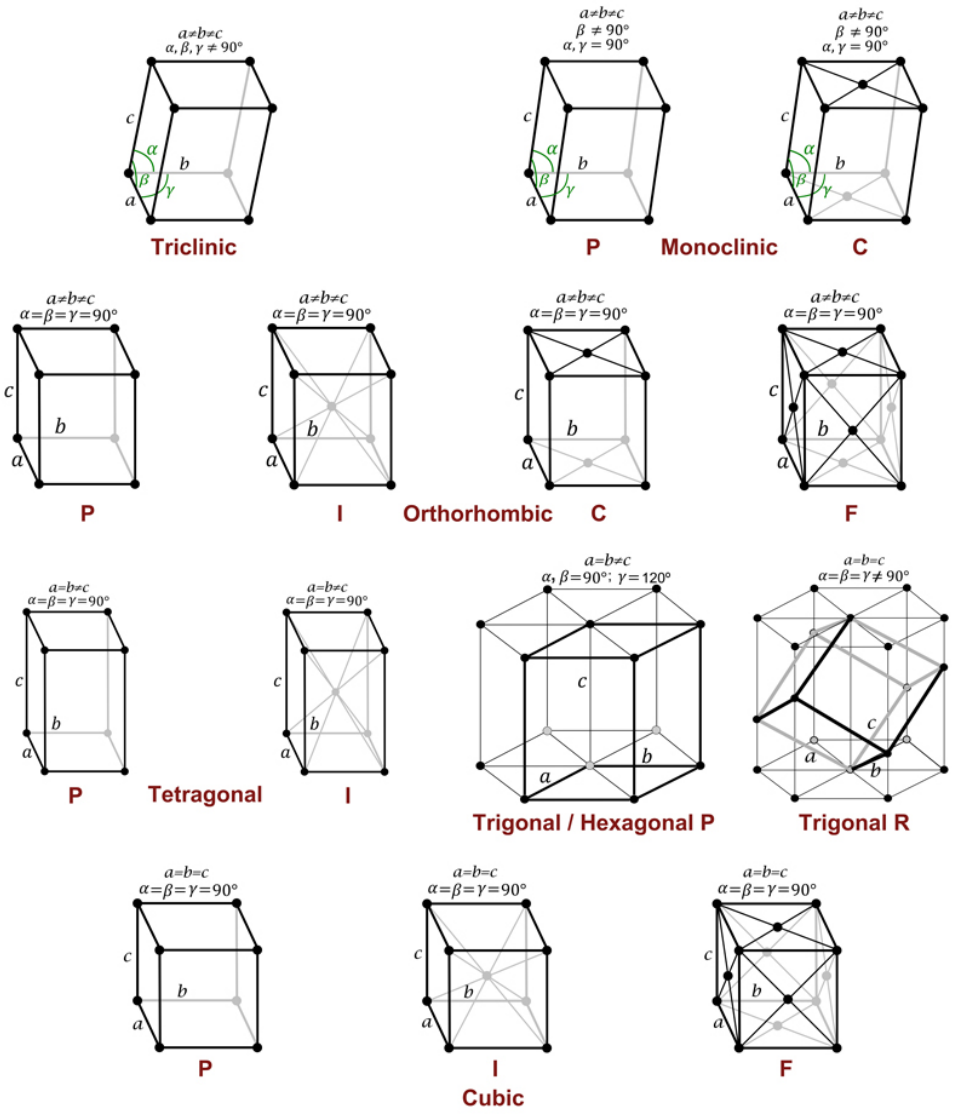

Source: (THE SYMMETRY. . . , 2019).

2.7 Quantum Espresso

The Quantum-ESPRESSO (Quantum-opEn-Source Package for Research in Electronic Structure, Simulation, and Optimization) package is a multipurpose and multi-platform software for *ab-initio* calculations of condensed matter systems (GIANNOZZI et al., 2020; GIANNOZZI et al., 2009). The calculus is based on density functional theory for describing electron-electron interactions, and a plane wave basis sets for the expansion of the electronic wave function, and a pseudopotential description of the electron-ion interaction (SCANDOLO et al., 2005).

The codes use periodic boundary conditions for the direct treatment of infinite crystal systems and an efficient convergence to extended aperiodic systems to the thermodynamic limit (GIANNOZZI et al., 2009).

It calculates the ground-state energy and Kohn-Sham orbitals for insulators, metals, and semiconductors, in any crystal structure, for many exchange-correlation functionals. It can perform various structural optimizations, and variable-cell molecular dynamics (GIANNOZZI et al., 2017).

3 METHODS

The Three minerals, $PdCuBiX_3$ (X represents the chalcogens, i.e., S, Se, or Te), have the same structure (orthorhombic), which contain three independent metal positions (Cu, Pd, and Bi) and three X positions, based on six atoms, show Fig. 3.1. The Cu site displays a strongly deformed tetrahedral coordination $[CuX_4]$. Palladium atoms show square-planar coordination, typical of the $4d^8$ electron configuration of Pd^{2+}. The $[PdX_4]$ squares are almost perfectly planar. Four X atoms surround bismuth atoms (VYMAZALOVÁ et al., 2020; LAUFEK et al., 2019).

Figura 3.1 – Crystal structure of $PdCuBiX_3$.

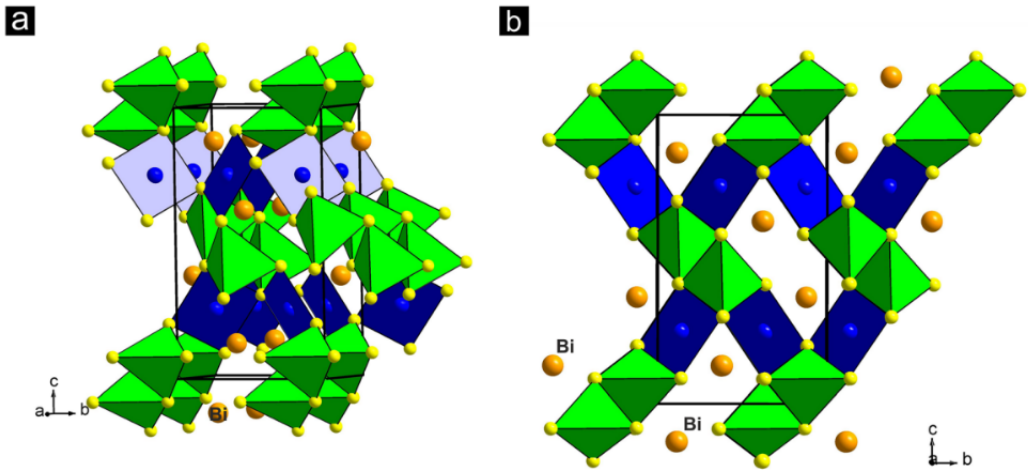

Label: (a) Inclined view; (b) view along the a axis. The $[CuX_4]$ tetrahedral and $[PdX_4]$ squares are highlighted (note that X in yellow represents the chalcogens, i.e., S, Se, or Te); Bi atoms are light orange.

Source: (VYMAZALOVÁ et al., 2020)

The DFT calculations of the solids ($PdCuBiX_3$ - X = S, Se or Te) were performed by Quantum-ESPRESSO (view section 2.7). And the exchange-correlation energy is evaluated within the Perdew–Zunger's LDA (LDA-PZ) (PERDEW; MCMULLEN; ZUNGER, 1981). The valence electron-ion interactions were considered by using norm-conserving pseudopotentials (TROULLIER; MARTINS, 1991). In the geometry relaxation, the residual force on the atoms was converged less than 2,57 meV/Å, the residual bulk stress less than 0.01 GPa, the energy cutoff to describe the electronic wave functions was 1,17 meV, and The Brillouin zone integration was performed within the Monkhorst–Pack scheme (PACK; MONKHORST, 1977), by using $6 \times 4 \times 2$ Gamma center k-point grids in the geometry optimization calculations.

Then, using the converged geometries under several pressures, the bulk modulus was calculated by a non-linear fit of the thermodynamic Equation of State (EOS). The equations used were the Murnaghan Equation of State:

$$E(V) = E_0 + K_0 V_0 \left[\frac{1}{K_0'(K_0'-1)} \left(\frac{V}{V_0} \right)^{1-K_0'} + \frac{1}{K_0'} \frac{V}{V_0} - \frac{1}{K_0'-1} \right], \tag{3.1}$$

and Birch–Murnaghan Isothermal Equation of State:

$$E(V) = E_0 + \frac{9V_0B_0}{16} \left\{ \left[\left(\frac{V_0}{V} \right)^{\frac{2}{3}} - 1 \right]^3 B_0' + \left[\left(\frac{V_0}{V} \right)^{\frac{2}{3}} - 1 \right]^2 \left[6 - 4 \left(\frac{V_0}{V} \right)^{\frac{2}{3}} \right] \right\}, \tag{3.2}$$

where $E(V)$ is the internal energy, E_0 is the initial energy at zero pressure and V_0 is its volume, V is the deformed volume, B_0 or K_0 is the bulk modulus, and B_0' or K_0' is the derivative of the bulk modulus with respect to pressure (MURNAGHAN, 1944; BIRCH, 1947).

Besides, the bulk modulus and its derivative are defined as:

$$B_0 = K_0 = -V \left(\frac{\partial P}{\partial V} \right)_T, \tag{3.3}$$

and

$$B_0' = K_0' = \left(\frac{\partial B_0}{\partial P} \right)_T, \tag{3.4}$$

where P is the pressure and T is the temperature.

Also, using the converged geometries under several pressures, was fitted the lattice parameters per pressure, and the relative percent deviation (relative error) is shown in the right y axis, defined by:

$$\%value = \frac{X - X_0}{X_0} \times 100, \tag{3.5}$$

where X is the lattice constant under some pressure of interest, and X_0 is the lattice constant under zero pressure.

Ultimately, the electronic structure and the Density Of States (DOS) were calculated for five pressure variations (-0,5 GPa, -0,25 GPa, 0 GPa, 0,25 GPa, and 0,5 GPa), with 8x6x4 k-point grids. In the calculation of the band structure, the points of symmetry of the Brillouin zone (K-path: $\Gamma - X - S - Y - \Gamma - Z - U - R - T - Z$) (SETYAWAN; CURTAROLO, 2010). Then, the pressure band gap variation was evaluated using the least square fit in the linear and

quadratic functions, respectively:

$$E(P) = bP + E(0), \tag{3.6}$$

and

$$E(P) = aP^2 + bP + E(0), \tag{3.7}$$

where energy E in eV, angular or linear coefficient b in eV/GPa (respectively), quadratic coefficient a in eV/GPa², and pressure P in GPa.

4 RESULTS AND DISCUSSIONS

The optimized lattice constants of minerals, $PdCuBiX_3$ (X = S, Se, or Te), are shown in Tab. 4.1 in the right column. On the left, have the experimental data taken from (LAUFEK et al., 2019) for $PdCuBiS_3$ and (VYMAZALOVÁ et al., 2020) for $PdCuBiSe_3$. Anyway, there is no DFT theoretical data of the three minerals in the literature to compare; and $PdCuBiTe_3$ needs the experimental data for comparison. The DFT simulations converged well with data close to the experimental data.

Tabela 4.1 – Comparison theoretical with experiment data.

Lattice Parameters	**Experimental Data**		**ab initio Data**		
	$PdCuBiS_3$	$PdCuBiSe_3$	$PdCuBiS_3$	$PdCuBiS_3$	$PdCuBiTe_3$
Norm of a	4.8847(8) Å	5,00520(10) Å	4,774 Å	4,886 Å	5,169 Å
Norm of b	7.5885(11) Å	7,9921(2) Å	7,565 Å	7,846 Å	8,122
Norm of c	12.8646(10) Å	13,5969(2) Å	12,562 Å	13,217 Å	13,675 Å
Volume	476.86(11) $Å^3$	543,90(2) $Å^3$	453,630 $Å^3$	506,786 $Å^3$	574,187 $Å^3$

Font: Author (2022).

The non-linear adjustment was fitted by the Birch-Murnaghan and Murnaghan equation of states (eq. 3.2 and eq. 3.1) on the same graph made with the data of the system's total energy and crystal volume obtained by several simulations of different pressures (Fig. 4.1). Each black dot on the graph represents a calculation made by the DFT. The red curve represents the fit using the Birch-Murnaghan equation (BM) and, the blue curve plotted represents the Murnaghan equation (MU) fit.

Figura 4.1 – Non-linear fitting Birch-Murnaghan and Murnaghan (EOS)

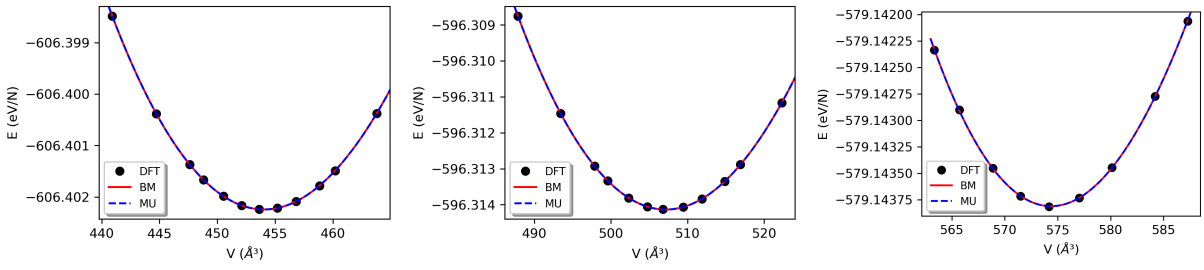

Label: (a) $PdCuBiS_3$; (b) $PdCuBiSe_3$; (c) $PdCuBiTe_3$.
Source: Author(2012).

Table 4.2 is represented the adjusted parameters of the Birch-Murnaghan Equation: B_0, B_0', V_0, and E_0 are the bulk modulus, the derivative of bulk modulus, initial volume, and initial energy, respectively. On the other hand, table 4.3 is represented the adjusted parameters of the

Murnaghan Equation: K_0, K_0', V_0, and E_0 are the bulk modulus, the derivative of bulk modulus, initial volume and initial energy, respectively.

Tabela 4.2 – Fitted Parameters Birch-Murnaghan Equation

Parameters	$PdCuBiS_3$	$PdCuBiSe_3$	$PdCuBiTe_3$
B_0 (GPa)	71,65(3)	53,02(3)	50,3(2)
B_0'	5,19(7)	3,74(8)	9,2(9)
V_0 (Å³)	454,042(3)	507,164(6)	574,38(3)
E_0 (eV/N)	−606,402242(4)	−596,314135(1)	−579,143812(3)

Source: Author(2012).

Tabela 4.3 – Fitted Parameters Murnaghan Equation

Parameters	$PdCuBiS_3$	$PdCuBiSe_3$	$PdCuBiTe_3$
K_0 (GPa)	71,64(3)	53,01(3)	50,3(2)
K_0'	5,15(7)	3,72(7)	9,2(1,1)
V_0 (Å³)	454,043(3)	507,165(5)	574,38(3)
E_0 (eV/N)	−606,402242153(5)	−596,314135(5)	−579,143811(3)

Source: Author(2012).

The bulk modulus (K or B) provides how much a substance is resistant to compression. The material's bulk modulus is the ratio of the change in pressure to the fractional volume compression. It's true that as a solid is experimentally compressed, it becomes more challenging to compress. That's why the non-linear fit.

Thus, you can see in the previous tables that the sulfur compost is more resistant to pressure. That is, it has a higher bulk modulus.

Another interesting fact is to know how the lattice parameters fluctuate under different pressures. Indeed Fig. 4.2 shows the parameters under several high pressures. Fig. 4.2(a) shows the norm of the lattice vector $\vec{a}$ in red, green, and blue circles for $PdCuBiS_3$ (sulfur from now on), $PdCuBiSe_3$ (selenium from now on) and $PdCuBiTe_3$ (tellurium from now on), respectively. Fig. 4.2(b) shows the norm of the lattice vector $\vec{b}$ in red, green, and blue squares for sulfur, selenium, and tellurium, respectively. And last but not least, Fig. 4.2(c) shows the norm of the lattice vector $\vec{c}$ in red, green, and blue triangles for sulfur, selenium, and tellurium, respectively.

Also, the bar to the right axle of the graphs shows the relative percentage values in red, blue, and green lines for sulfur, tellurium, and selenium, respectively. they were calculated in relation to a_0 which corresponds to the value of the norm of $\vec{a}$, or just a, under zero pressure.

It can be seen in Fig. 4.2(a) that the lattice vector $\vec{a}$ for sulfur is more compressible. Fig. 4.2(b) the network vector $\vec{b}$ of Selenium undergoes a further reduction. The same happens

Figura 4.2 – Lattices parameters under high-pressure

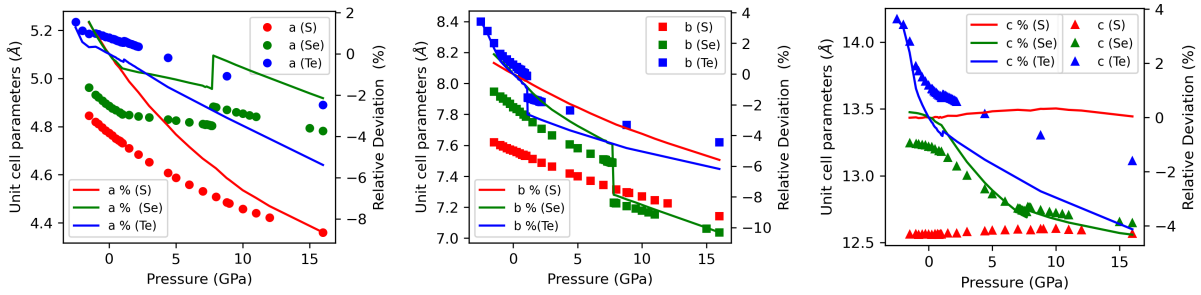

Label: (a) norm of a (circles) and relative deviation (lines) for S, Se, and Te; (b) norm of b (squares) and relative deviation (lines) for S, Se, and Te; (c) norm of c (triangles) and relative deviation (lines) for S, Se, and Te.

Source: Author(2012).

in Fig. 4.2(c) as a lattice vector $\vec{c}$ of selenium. It can be noted that for sulfur, there are no perceptible variations in this pressure range. It is noteworthy that the relative percentage value is negative for compression and positive for the expansion of the solid.

The main difference between conductors, semiconductors, and insulators lies in their electronic structure or band structure. And the main factor for differentiating between the three types of electronic conduction is the evaluation of the band gap dimension. So, in the figures: Fig. 4.3, Fig. 4.4, Fig. 4.5, show the band structure and DOS in the region close to the band gap of the interest materials at -0,5 GPa, 0 GPa, and 0,5 GPa, respectively. The DOS describes the number of states that are to be occupied by the electrons at each energy. The Fermi energy was set to 0 eV, dashed red line in the cited figures.

At -0,5 GPa, the sulfur compound and selenium compound, represented by the Fig. 4.3(a) and Fig. 4.3(b), is a semiconductor with an indirect band gap of the 0,5712 eV and 0,4023 eV, respectively. Still, at -0,5 GPa, the tellurium compound, represented by Fig. 4.3(c), is a conductor (without a band gap).

At the pressure of 0 GPa, the sulfur compound and selenium compound, represented by Fig. 4.4(a) and Fig. 4.4(b), is a semiconductor with an indirect band gap of the 0,5732 eV and 0,4100 eV, respectively. Still, at 0 GPa, the tellurium compound, represented by Fig. 4.4(c), is a metal.

Now similarly, at the pressure of 0,50 GPa, the sulfur compound and selenium compound, represented by the Fig. 4.5(a) and Fig. 4.5(b), it is a semiconductor with an indirect band gap of the 0,5794 eV and 0,4023 eV, respectively. Still, at 0,5 GPa, the tellurium compound, represented by Fig. 4.5(c), is a metal.

Figura 4.3 – Band Structure and DOS calculation at -0,50 GPa

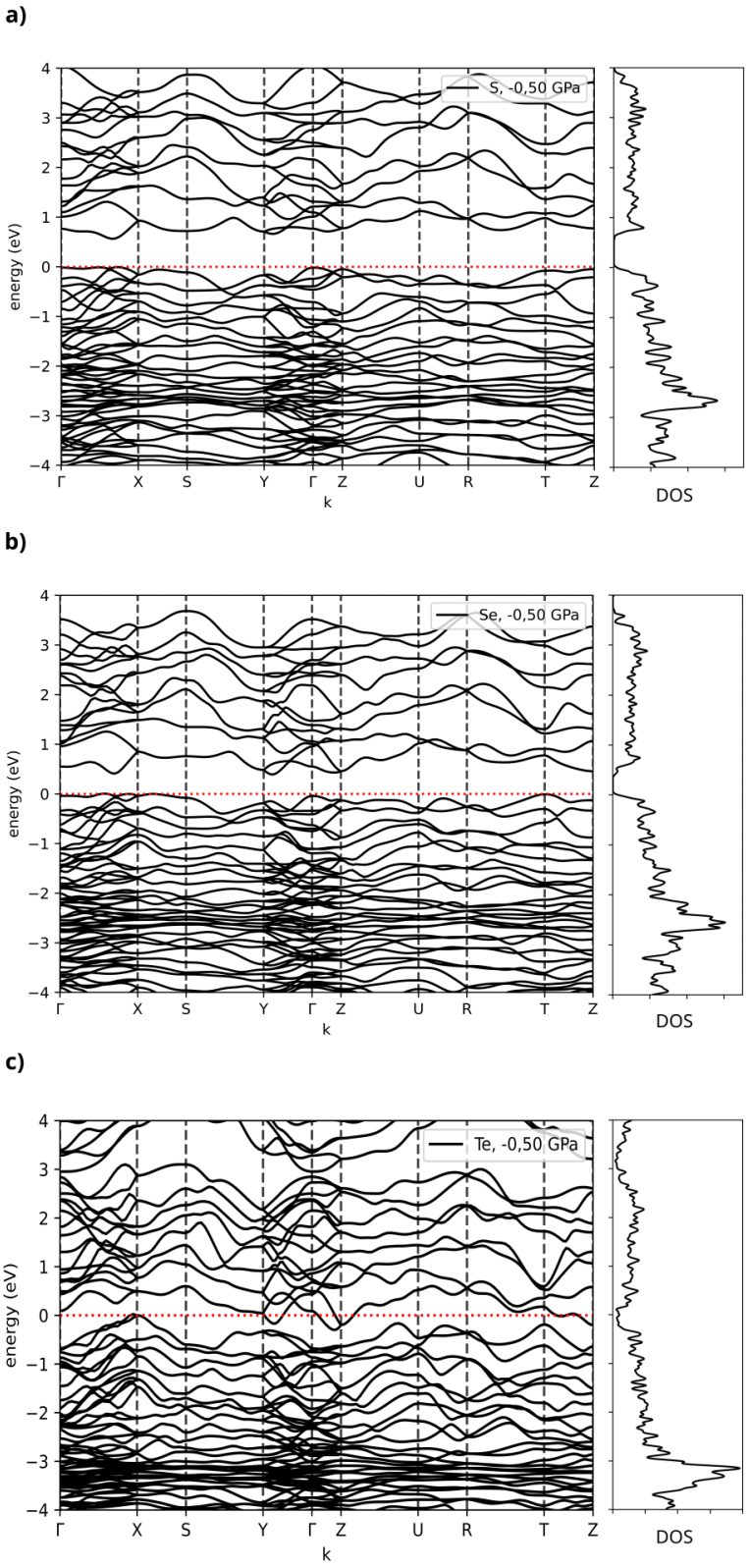

Label: (a) $PdCuBiS_3$; (b) $PdCuBiSe_3$; (c) $PdCuBiTe_3$.

Source: Author(2012).

Figura 4.4 – Band Structure and DOS calculation at 0 GPa

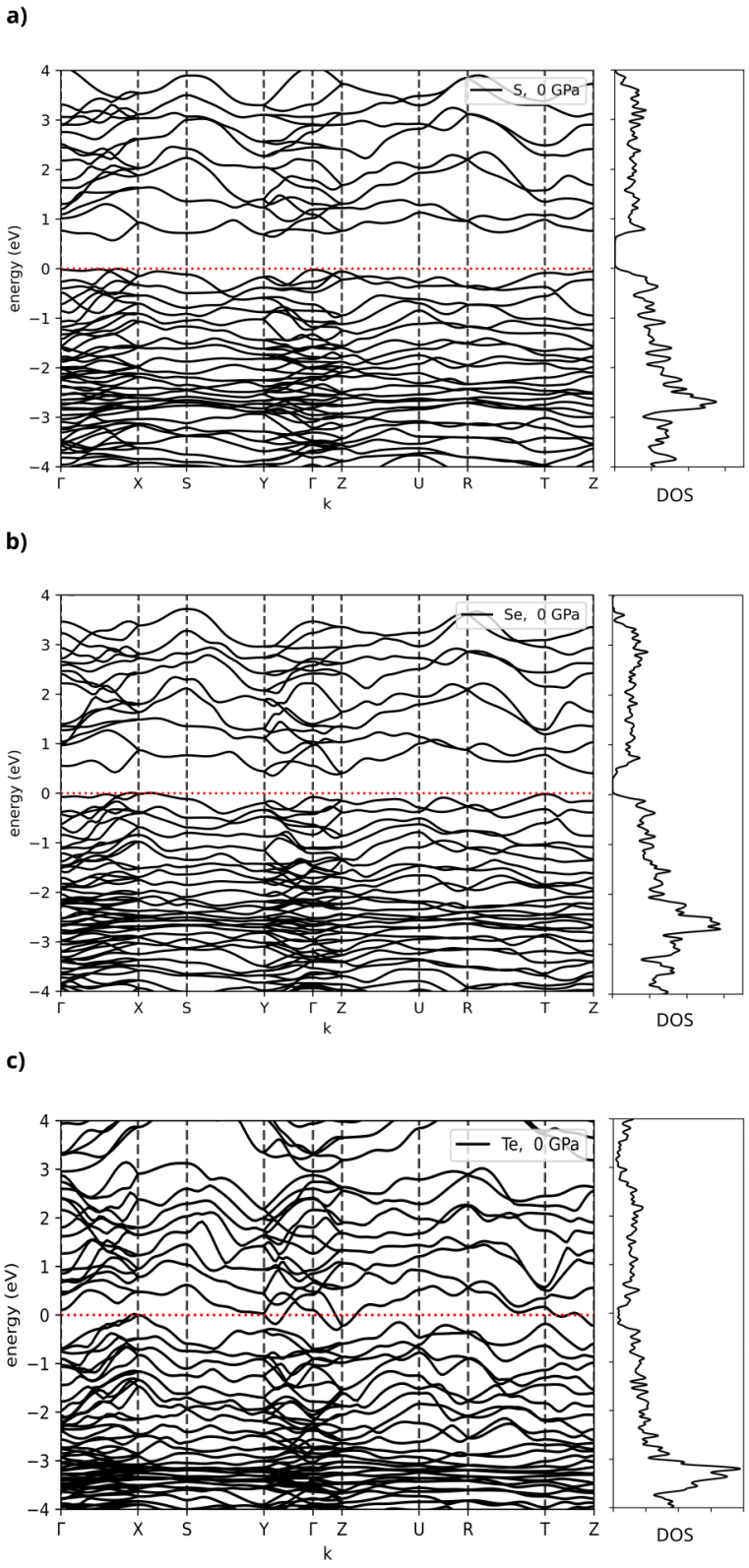

Label: (a) $PdCuBiS_3$; (b) $PdCuBiSe_3$; (c) $PdCuBiTe_3$.

Source: Author(2012).

Figura 4.5 – Band Structure and DOS calculation at 0,50 GPa

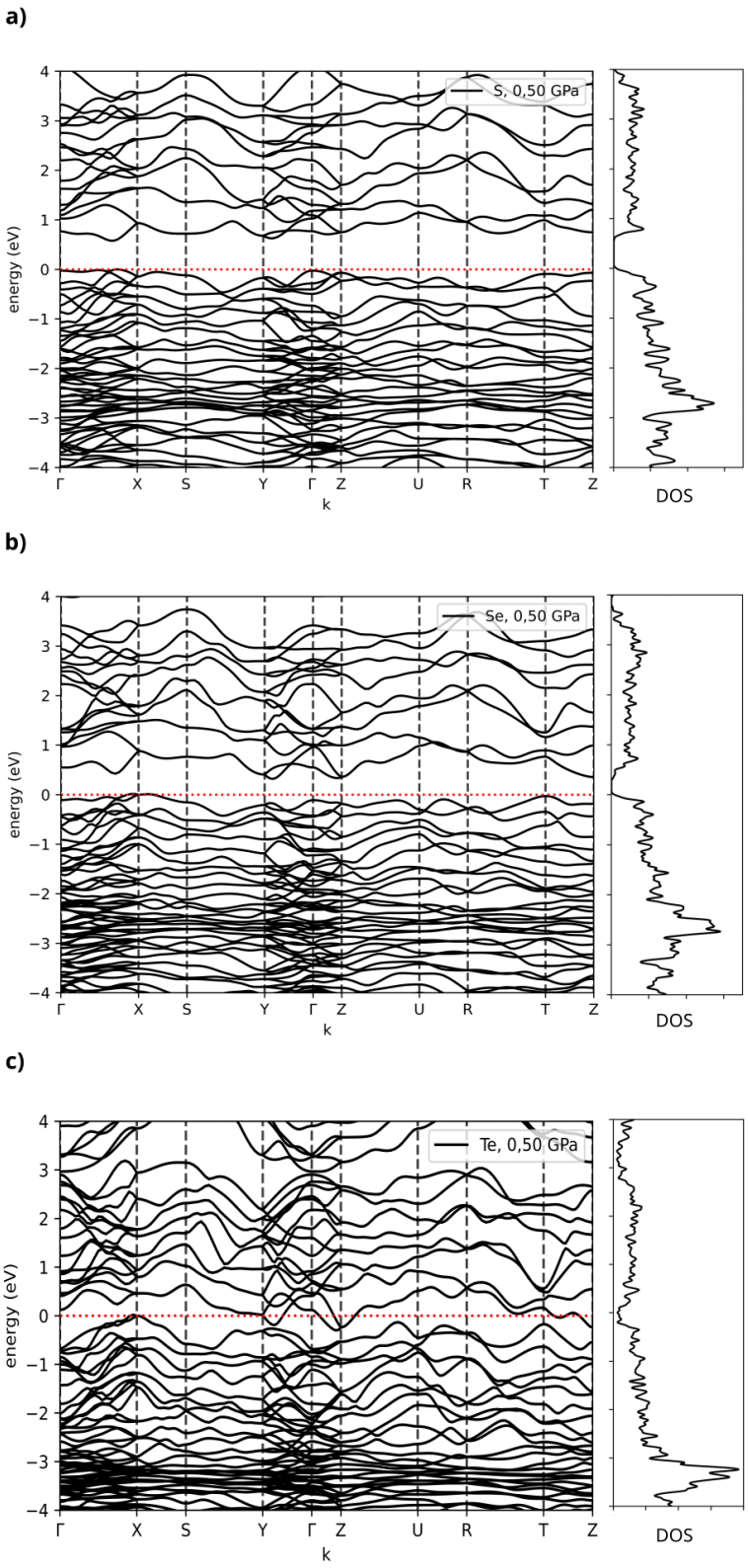

Label: (a) $PdCuBiS_3$; (b) $PdCuBiSe_3$; (c) $PdCuBiTe_3$.

Source: Author(2012).

Similar results were expected from interested materials under such pressures, causing only a slight variation in the band gap in semiconductor materials, i.e., $PdCuBiS_3$ and $PdCuBiSe_3$. To better understand the variation of the band gap by the pressure of these minerals, a curve fits according to eq. 3.6 (dashed blue line) and eq. 3.7 (dashed red line) was done, see the Fig. 4.6 and Fig. 4.7.

Figura 4.6 – The band gap by pressure quadratic and linear fits of Sulfur

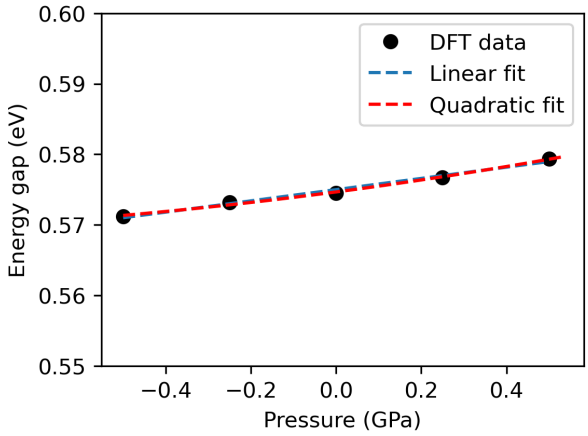

Source: Author(2012).

Figura 4.7 – The band gap by pressure quadratic and linear fits of Selenium

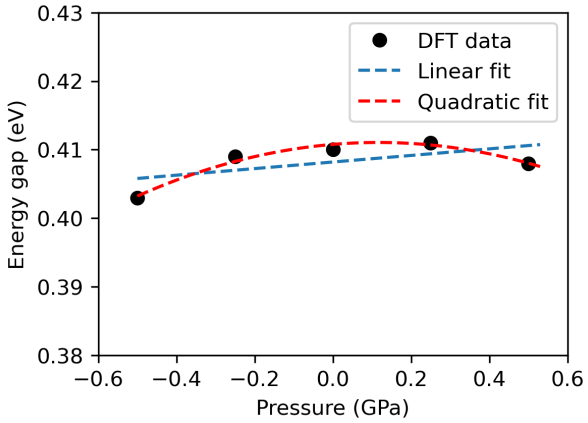

Source: Author(2012).

Fig. 4.6 shows that both equations, linear and quadratic, describe well the increase in the band gap linear variation. In Fig 4.7, the best fit is the quadratic curve, indicating the nonlinearity of the data.

The pressure coefficients derived from both fittings are given in Tab. 4.4 for comparison.

Tabela 4.4 – Pressure coefficients for the fundamental band gap

Minerals	**a** $(eV/GPa^2 \times 10^{-3})$	**b** $(eV/GPa \times 10^{-3})$	**E(0)** $(eV \times 10^{-3})$
`Sulfur (linear)`	-	$7,9(6)$	$575,0(2)$
`Sulfur (quadratic)`	$2(1)$	$7,9(4)$	$574,6(2)$
`Selenium (linear)`	-	$5(3)$	$408(1)$
`Selenium (quadratic)`	$-20(3)$	$5(1)$	$410,7(5)$

Source: Author(2012).

5 CONCLUSIONS AND FUTURE PERSPECTIVES

Under zero pressure, the calculated values for the lattice parameters, a b and c, the unit cell volume, and the atomic positions of $PdCuBiS_3$ and $PdCuBiSe_3$ are in good agreement with experimental values for an initial study. The unit cell volume had a decrease of approximately 4,8 % and 6,8 %, respectively. The $PdCuBiTe_3$ has no experimental data for comparison.

The materials were subjected to pressures ranging from 0 to 15 GPa to obtain their mechanical properties. In addition, the materials were subjected to pressures of 100 GPa, in order to study their structural alterations, which are still under analysis.

Electronic structure calculations under the calculated pressures in the window -0,5 to 0,5 GPa demonstrated that $PdCuBiS_3$ and $PdCuBiSe_3$ are semiconductors with an indirect band gap, and $PdCuBiTe_3$ is metallic.

A proposal for future work would be the synthesis of Te compost and the experimental study of the electronic, structural and mechanical properties of these materials ($PdCuBiS_3$, $PdCuBiSe_3$ and $PdCuBiTe_3$).

REFERÊNCIAS

ANDREONI, W.; CURIONI, A. New advances in chemistry and materials science with CPMD and parallel computing. **Parallel Computing**, v. 26, n. 7, p. 819–842, 2000. Disponível em: <https://www.sciencedirect.com/science/article/pii/S0167819100000144>.

ANZELLINI, S. et al. Thermal equation of state of ruthenium characterized by resistively heated diamond anvil cell. **Scientific reports**, Nature Publishing Group, v. 9, n. 1, p. 1–11, 2019.

AROYO, M. I. **International Tables for Crystallography Volume A: Space-group symmetry**. Second online edition. International Union of Crystallography, 5 Abbey Square, Chester CH1 2HU, England: Wiley Online Library, 2016.

ASHCROFT, N. W.; MERMIN, N. D. et al. **Solid state physics**. [S.l.]: holt, rinehart and winston, new york London, 1976.

AVERILL, B. A. **Crystalline and Amorphous Solids**. 2021. Access on February 03, 2022. Disponível em: <https://chem.libretexts.org/@go/page/6402>.

BASEDEN, K. A.; TYE, J. W. Introduction to density functional theory: Calculations by hand on the helium atom. **Journal of Chemical Education**, v. 91, n. 12, p. 2116–2123, 2014. Disponível em: <https://doi.org/10.1021/ed5004788>.

BECKER, J. A. Percy w. bridgman. **Physics Today**, v. 14, n. 10, p. 78–78, 1961. Disponível em: <https://doi.org/10.1063/1.3057180>.

BIRCH, F. Finite elastic strain of cubic crystals. **Physical Review**, American Physical Society, v. 71, p. 809–824, Jun 1947. Disponível em: <https://link.aps.org/doi/10.1103/PhysRev.71.809>.

BORN, M.; OPPENHEIMER, R. Zur quantentheorie der molekeln. **Annalen der Physik**, v. 389, n. 20, p. 457–484, 1927. Disponível em: <https://onlinelibrary.wiley.com/doi/abs/10.1002/andp.19273892002>.

BRIDGMAN, P. W. A complete collection of thermodynamic formulas. **Physical Review**, American Physical Society, v. 3, p. 273–281, Apr 1914. Disponível em: <https://link.aps.org/doi/10.1103/PhysRev.3.273>.

BRITANNICA. **Sulfosalt**. Encyclopedia Britannica, 2018. Accessed July 19, 2022. Disponível em: <https://www.britannica.com/science/sulfosalt>.

BROWN, J. M.; MCQUEEN, R. G. Phase transitions, grüneisen parameter, and elasticity for shocked iron between 77 gpa and 400 gpa. **Journal of Geophysical Research: Solid Earth**, v. 91, n. B7, p. 7485–7494, 1986. Disponível em: <https://agupubs.onlinelibrary.wiley.com/doi/abs/10.1029/JB091iB07p07485>.

BUDZIANOWSKI, A.; KATRUSIAK, A. High-pressure crystallographic experiments with a ccd-detector. In: **High-pressure crystallography**. [S.l.]: Springer, 2004. p. 101–112.

CABRAL, A. R.; LIESSMANN, W.; LEHMANN, B. Gold and palladium minerals (including empirical pdcubise3) from the former roter bär mine, st. andreasberg, harz mountains, germany: a result of low-temperature, oxidising fluid overprint. **Mineralogy and Petrology**, Springer, v. 109, n. 5, p. 649–657, 2015.

CHAO, E. C. T.; SHOEMAKER, E. M.; MADSEN, B. M. First natural occurrence of coesite. **Science**, American Association for the Advancement of Science, v. 132, n. 3421, p. 220–222, 1960. Disponível em: <https://science.sciencemag.org/content/132/3421/220>.

CHELIKOWSKY, J. R. **Introductory Quantum Mechanics with MATLAB: For Atoms, Molecules, Clusters, and Nanocrystals**. [S.l.]: John Wiley & Sons, 2019.

CLARK, S. J. et al. First principles methods using castep. **Zeitschrift für kristallographie-crystalline materials**, De Gruyter Oldenbourg, v. 220, n. 5-6, p. 567–570, 2005.

COHEN, A. J.; MORI-SáNCHEZ, P.; YANG, W. Challenges for density functional theory. **Chemical Reviews**, v. 112, n. 1, p. 289–320, 2012. PMID: 22191548. Disponível em: <https://doi.org/10.1021/cr200107z>.

COHEN-TANNOUDJI, C. et al. **Quantum Mechanics (2 vol. set)**. [S.l.]: Wiley-Interscience, 2006.

DOVESI, R. et al. Quantum-mechanical condensed matter simulations with crystal. **Wiley Interdisciplinary Reviews: Computational Molecular Science**, Wiley Online Library, v. 8, n. 4, p. e1360, 2018.

DUTTA, U. et al. Pressure-induced superconductivity in semimetallic $1t-\text{tite}_2$ and its persistence upon decompression. **Physical Review**, American Physical Society, v. 97, p. 060503, Feb 2018. Disponível em: <https://link.aps.org/doi/10.1103/PhysRevB.97.060503>.

DUTTA, U. et al. Infrared spectroscopic measurements of structural transition and charge dynamics in $1T-\text{tite}_2$ under pressure. **Physical Review**, American Physical Society, v. 99, p. 125105, Mar 2019. Disponível em: <https://link.aps.org/doi/10.1103/PhysRevB.99.125105>.

ECHENIQUE, P.; ALONSO, J. L. A mathematical and computational review of hartree–fock SCF methods in quantum chemistry. **Molecular Physics**, Taylor & Francis, v. 105, n. 23-24, p. 3057–3098, 2007. Disponível em: <https://doi.org/10.1080/00268970701757875>.

FERMI, E. Statistical method to determine some properties of atoms. **Rend. Accad. Naz. Lincei**, v. 6, n. 602-607, p. 5, 1927.

FLEISCHER, M. New mineral names: Uralborite, pentahydroborite. **American Mineralogist: Journal of Earth and Planetary Materials**, Mineralogical Society of America, v. 47, n. 11-12, p. 1482–1485, 1962. Disponível em: <http://www.minsocam.org/ammin/AM47/AM47_1482.pdf>.

FOCK, V. Selfconsistent field “mit austausch für natrium. **Zeitschrift für Physik**, Springer, v. 62, n. 11, p. 795–805, 1930.

Froese Fischer, C. General hartree-fock program. **Computer Physics Communications**, v. 43, n. 3, p. 355–365, 1987. ISSN 0010-4655. Disponível em: <https://www.sciencedirect.com/science/article/pii/0010465587900531>.

GASSER, T. M. et al. Structural characterization of ice XIX as the second polymorph related to ice VI. **Nature Communications**, Nature Publishing Group, v. 12, n. 1, p. 1–10, 2021. Disponível em: <https://rdcu.be/cuI0w>.

GAVEZZOTTI, A. Efficient computer modeling of organic materials. the atom–atom, coulomb–london–pauli (AA-CLP) model for intermolecular electrostatic-polarization, dispersion and repulsion energies. **New Journal of Chemistry**, Royal Society of Chemistry, v. 35, n. 7, p. 1360–1368, 2011.

GIANNOZZI, P. et al. Advanced capabilities for materials modelling with Quantum ESPRESSO. **Journal of Physics: Condensed Matter**, IOP Publishing, v. 29, n. 46, p. 465901, 2017. Disponível em: <https://dx.doi.org/10.1088/1361-648X/aa8f79>.

GIANNOZZI, P. et al. QUANTUM ESPRESSO: a modular and open-source software project for quantum simulations of materials. **Journal of Physics: Condensed Matter**, IOP Publishing, v. 21, n. 39, p. 395502, sep 2009. Disponível em: <https://doi.org/10.1088/0953-8984/21/39/395502>.

GIANNOZZI, P. et al. Quantum ESPRESSO toward the exascale. **The Journal of Chemical Physics**, v. 152, n. 15, p. 154105, 2020. Disponível em: <https://doi.org/10.1063/5.0005082>.

HAMMES-SCHIFFER, S. A conundrum for density functional theory. **Science**, v. 355, n. 6320, p. 28–29, 2017. Disponível em: <https://www.science.org/doi/abs/10.1126/science.aal3442>.

HAN, Y. et al. Integrated microcircuit on a diamond anvil for high-pressure electrical resistivity measurement. **Applied Physics Letters**, v. 86, n. 6, p. 064104, 2005. Disponível em: <https://doi.org/10.1063/1.1863444>.

HARRISON, N. An introduction to density functional theory. **Nato Science Series Sub Series III Computer and Systems Sciences**, IOS PRESS, v. 187, p. 45–70, 2003.

HARTREE, D. R. A mecânica ondulatória de um Átomo com campo central não coulombiano. parte II. some results and discussion. **Mathematical Proceedings of the Cambridge Philosophical Society**, v. 24, n. 1, p. 111–132, 1928.

HAZEN, R. M.; HAZEN, R. M. **The diamond makers**. [S.l.]: Cambridge University Press, 1999.

HELLMANN, H. A new approximation method in the problem of many electrons. **The Journal of Chemical Physics**, American Institute of Physics, v. 3, n. 1, p. 61–61, 1935.

HOHENBERG, P.; KOHN, W. Inhomogeneous electron gas. **Physical review**, APS, v. 136, n. 3B, p. B864, 1964. Disponível em: <https://journals.aps.org/pr/abstract/10.1103/PhysRev.136.B864>.

HUANG, Y. et al. Pressure-induced band structure evolution of halide perovskites: A first-principles atomic and electronic structure study. **The Journal of Physical Chemistry C**, v. 123, n. 1, p. 739–745, 2019. Disponível em: <https://doi.org/10.1021/acs.jpcc.8b11500>.

IFIMAC. **First Principles Simulations and Modeling**. [201–?]. Accessed July 21, 2022. Disponível em: <https://www.ifimac.uam.es/first-principles-simulations-and-modeling/>.

KANG, M. et al. Electrical characterization of multilayer hfse2 field-effect transistors on sio2 substrate. **Applied Physics Letters**, v. 106, n. 14, p. 143108, 2015. Disponível em: <https://doi.org/10.1063/1.4917458>.

KATRUSIAK, A. High-pressure crystallography. **Acta Crystallographica Section A: Foundations of Crystallography**, International Union of Crystallography, v. 64, n. 1, p. 135–148, 2008.

KITTEL, C.; MCEUEN, P.; MCEUEN, P. **Introduction to solid state physics**. [S.l.]: Wiley New York, 1996.

KOHN, W. Nobel lecture: Electronic structure of matter—wave functions and density functionals. **Reviews of Modern Physics**, APS, v. 71, n. 5, p. 1253, 1999.

KOHN, W.; SHAM, L. J. Self-consistent equations including exchange and correlation effects. **Physical review**, APS, v. 140, n. 4A, p. A1133, 1965.

KUHS, W. The high pressure crystallography of gas hydrates. In: **High-Pressure Crystallography**. [S.l.]: Springer, 2004. p. 475–494.

LAUFEK, F. et al. Crystal structure and transport properties of cupdbis3. **Journal of Alloys and Compounds**, Elsevier, v. 792, p. 983–987, 2019.

LI, R. et al. Pressure effect on electronic and excitonic properties of purely j-aggregated monolayer organic semiconductor. **The Journal of Physical Chemistry Letters**, v. 11, n. 15, p. 5896–5901, 2020. PMID: 32631059. Disponível em: <https://doi.org/10.1021/acs.jpclett.0c01809>.

LOBATO, R. L. M. **Estrutura Eletrônica e Estabilidade de a-Grafinos; Absorção Óptica em Marcadores Biológicos; Domínios de Potenciais Eletrostáticos na Superfície de Grafite**. 152 p. Tese (Doutorado) — Departamento de Física, Universidade Federal de Minas Gerais, Belo Horizonte - MG, 30 de janeiro de 2015.

LOWER, S. **States of matter - Introduction**. 2017. Access on February 03, 2022. Disponível em: <http://www.chem1.com/acad/webtext/states/states.html#SEC4>.

MACKENZIE, C. F. et al. Crystalexplorer model energies and energy frameworks: extension to metal coordination compounds, organic salts, solvates and open-shell systems. **IUCrJ**, International Union of Crystallography, v. 4, n. 5, p. 575–587, 2017.

MAO, H.-K. et al. Recent advances in high-pressure science and technology. **Matter and Radiation at Extremes**, v. 1, n. 1, p. 59–75, 2016. Disponível em: <https://aip.scitation.org/doi/abs/10.1016/j.mre.2016.01.005>.

MAO, H. K. et al. Phonon density of states of iron up to 153 gigapascals. **Science**, American Association for the Advancement of Science, v. 292, n. 5518, p. 914–916, 2001. ISSN 0036-8075. Disponível em: <https://science.sciencemag.org/content/292/5518/914>.

METEOR Crater. Wikipedia, the free encyclopedia, [2021?]. Access on August 17, 2020. Disponível em: <https://en.wikipedia.org/wiki/Meteor_Crater>.

MURNAGHAN, F. D. The compressibility of media under extreme pressures. **Proceedings of the National Academy of Sciences**, National Academy of Sciences, v. 30, n. 9, p. 244–247, 1944. ISSN 0027-8424. Disponível em: <https://www.pnas.org/content/30/9/244>.

NELSON, S. A. **Introduction and Symmetry Operations**. 2013. Access on February 03, 2022. Disponível em: <https://www.tulane.edu/~sanelson/eens211/introsymmetry.htm#:~:text=There\%20are\%203\%20types\%20of,rotation\%2C\%20reflection\%2C\%20and\%20inversion.>

NEWITT, B. M. Percy williams bridgman, 1882-1961. **Biographical Memoirs of Fellows of the Royal Society**, v. 8, p. 26–40, 1962. Disponível em: <https://royalsocietypublishing.org/doi/10.1098/rsbm.1962.0003>.

OGANOV, A. R.; BRODHOLT, J. P.; PRICE, G. D. Ab initio theory of phase transitions and thermoelasticity of minerals. In: **Energy Modelling in Minerals**. Mineralogical Society of Great Britain and Ireland, 2002. ISBN 9789634635666. Disponível em: <https://doi.org/10.1180/EMU-notes.4.4>.

PACK, J. D.; MONKHORST, H. J. Special points for brillouin-zone integrations —a reply. **Physical Review**, American Physical Society, v. 16, p. 1748–1749, Aug 1977. Disponível em: <https://link.aps.org/doi/10.1103/PhysRevB.16.1748>.

PARR, R. G. Density functional theory of atoms and molecules. In: **Horizons of quantum chemistry**. [S.l.]: Springer, 1980. p. 5–15.

PATTERSON, J. R. et al. Electrical and mechanical properties of C_{70} fullerene and graphite under high pressures studied using designer diamond anvils. **Physical Review**, American Physical Society, v. 85, p. 5364–5367, Dec 2000. Disponível em: <https://link.aps.org/doi/10.1103/PhysRevLett.85.5364>.

PERDEW, J.; MCMULLEN, E.; ZUNGER, A. Density-functional theory of the correlation energy in atoms and ions: a simple analytic model and a challenge. **Physical Review A**, APS, v. 23, n. 6, p. 2785, 1981.

RAHMAN, M. T.; HAQUE, E.; HOSSAIN, M. A. Elastic, electronic and thermoelectric properties of sr3mn (m = sb, bi) under pressure. **Journal of Alloys and Compounds**, v. 783, p. 593–600, 2019. ISSN 0925-8388. Disponível em: <https://www.sciencedirect.com/science/article/pii/S0925838818349016>.

RÖSSLER, U. **Solid state theory: an introduction**. [S.l.]: Springer Science & Business Media, 2009.

RYCHKOV, D. A. A short review of current computational concepts for high-pressure phase transition studies in molecular crystals. **Crystals**, v. 10, n. 2, 2020. ISSN 2073-4352. Disponível em: <https://www.mdpi.com/2073-4352/10/2/81>.

SCANDOLO, S. et al. First-principles codes for computational crystallography in the quantum-espresso package. **Zeitschrift für Kristallographie - Crystalline Materials**, v. 220, n. 5-6, p. 574–579, 2005. Disponível em: <https://doi.org/10.1524/zkri.220.5.574.65062>.

SETYAWAN, W.; CURTAROLO, S. High-throughput electronic band structure calculations: Challenges and tools. **Computational Materials Science**, v. 49, n. 2, p. 299–312, 2010. ISSN 0927-0256. Disponível em: <https://www.sciencedirect.com/science/article/pii/S0927025610002697>.

SHIMIZU, H. et al. In situ observations of high-pressure phase transformations in a synthetic methane hydrate. **The Journal of Physical Chemistry B**, ACS Publications, v. 106, n. 1, p. 30–33, 2002.

SLATER, J. C. A simplification of the hartree-fock method. **Physical Review**, American Physical Society, v. 81, p. 385–390, Feb 1951. Disponível em: <https://link.aps.org/doi/10.1103/PhysRev.81.385>.

SYMMETRY in Crystallography. Dept. of Chemistry & Biochemistry. University of Oklahoma: [s.n.], 2019. Access on February 03, 2022. Disponível em: <http://xrayweb.chem.ou.edu/notes/symmetry.html>.

THE SYMMETRY of crystals. Representation of Bravais lattices. 2019. Access on February 03, 2022. Disponível em: <https://www.xtal.iqfr.csic.es/Cristalografia/parte_03_4-en.html>.

THOMAS, L. H. The calculation of atomic fields. **Mathematical Proceedings of the Cambridge Philosophical Society**, Cambridge University Press, v. 23, n. 5, p. 542–548, 1927.

THOMAS, S. P. et al. Accurate lattice energies for molecular crystals from experimental crystal structures. **Journal of chemical theory and computation**, ACS Publications, v. 14, n. 3, p. 1614–1623, 2018.

TROULLIER, N.; MARTINS, J. L. Efficient pseudopotentials for plane-wave calculations. **Physical Review B**, American Physical Society, v. 43, p. 1993–2006, Jan 1991. Disponível em: <https://link.aps.org/doi/10.1103/PhysRevB.43.1993>.

TSE, J. S. A chemical perspective on high pressure crystal structures and properties. **National Science Review**, v. 7, n. 1, p. 149–169, 10 2019. ISSN 2095-5138. Disponível em: <https://doi.org/10.1093/nsr/nwz144>.

VELISAVLJEVIC, N.; VOHRA, Y. K. Bioceramic hydroxyapatite at high pressures. **Applied Physics Letters**, v. 82, n. 24, p. 4271–4273, 2003. Disponível em: <https://doi.org/10.1063/1.1584076>.

VYMAZALOVÁ, A. et al. Roterbärite, $PdCuBiSe_3$, a new mineral species from the roter bär mine, harz mountains, germany. **Mineralogy and Petrology**, Springer, v. 114, p. 443–451, 2020. Disponível em: <https://doi.org/10.1007/s00710-020-00703-1>.

VYMAZALOVÁ, A. et al. Roterbärite, IMA 2019-043. CNMNC newsletter no. 51. **Mineralogical Magazine**, v. 83, p. 757–761, 2019.

WANG, J. et al. $C_3H_6N_6$ doping effect of synthetic diamond under high pressure and high temperature. **International Journal of Refractory Metals and Hard Materials**, v. 87, p. 105150, 2020. ISSN 0263-4368. Disponível em: <https://www.sciencedirect.com/science/article/pii/S0263436819307474>.

WHAT Are Bravais Lattices? (Definition, Types, Examples). [201–?]. Access on February 03, 2022. Disponível em: <https://msestudent.com/what-are-bravais-lattices-definition-types-examples/>.

WIKEMEDIA Commons. Wikipedia, the free encyclopedia, 2006. Access on August 11, 2022. Disponível em: <https://commons.wikimedia.org/w/index.php?curid=10227075>.

ZHANG, L. et al. Materials discovery at high pressures. **Nature Reviews Materials**, Nature Publishing Group, v. 2, n. 4, p. 1–16, 2017. Disponível em: <https://doi.org/10.1038/natrevmats.2017.5>.

ZHANG, X. et al. Semiconductor-to-metal transition in HfSe_2 under high pressure. **Journal of Alloys and Compounds**, v. 867, p. 158923, 2021. ISSN 0925-8388. Disponível em: <https://www.sciencedirect.com/science/article/pii/S0925838821003303>.

ZIMAN, J. M. **Principles of the Theory of Solids**. [S.l.]: Cambridge university press, 1972.